

HOSTED BY



ELSEVIER

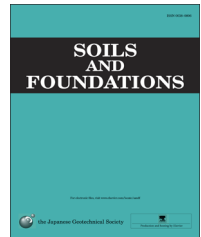


CrossMark

The Japanese Geotechnical Society

Soils and Foundations

www.sciencedirect.com
journal homepage: www.elsevier.com/locate/sandf



Study on the pore water pressure dissipation method as a liquefaction countermeasure using soil–water coupled finite deformation analysis equipped with a macro-element method

Toshihiro Noda^{a,*}, Shotaro Yamada^b, Toshihiro Nonaka^a, Mutsumi Tashiro^b

^aDisaster Mitigation Research Center, Nagoya University, Nagoya, Japan

^bDepartment of Civil Engineering, Nagoya University, Nagoya, Japan

Received 7 August 2014; received in revised form 13 March 2015; accepted 13 May 2015

Available online 26 September 2015

Abstract

A numerical simulation of the pore water pressure dissipation method was performed using the *GEOASIA* soil–water coupled finite deformation analysis code, which is capable of accounting for inertial forces, together with the elasto-plastic constitutive SYS Cam-clay model based on the soil skeleton structure concept, with the goal of quantitatively assessing the effects of this method as a countermeasure to liquefaction. At the same time, an effort was made to improve/enhance the calculation efficiency of the *GEOASIA* analysis code by incorporating a macro-element method, which up to this point has only been applied to consolidation problems. The main findings of this study are as follows: (1) the macro-element method is capable of yielding highly accurate approximations even for dynamic problems, (2) the method is capable of reproducing the suppression effect of the increase in pore water pressure associated with the pore water pressure dissipation method, even when a relatively coarse mesh is used, (3) the method is capable of reproducing the suppression effect of the decrease in effective stress due to the pore water pressure dissipation method, along with the resulting reduction in shear stiffness, lateral ground movement, and settlement and (4) it is possible to efficiently design the pore water pressure dissipation method with this method by first performing calculations using a 1-D mesh to determine the effective drain spacing prior to performing calculations using 2-D or 3-D meshes.

© 2015 The Japanese Geotechnical Society. Production and hosting by Elsevier B.V. All rights reserved.

Keywords: Pore water pressure dissipation method; Liquefaction countermeasure; Soil–water coupled analysis; Macro-element method

1. Introduction

In the pore water pressure dissipation method, liquefaction during earthquakes is inhibited by suppressing the increase in pore water pressure by means of the installation of vertical drains. The trade-off for this method is that some degree of ground surface settlement due to compaction must be allowed

for. Accordingly, in addition to the question of whether or not the method can be used to prevent liquefaction, it is important to be able to predict the degree of deformation that will occur as a result of ground compaction. The primary objective of this study is to employ a soil–water coupled analysis to quantitatively predict the effects, including the degree of ground deformation, of the pore water pressure dissipation method as a countermeasure to liquefaction.

A survey of the existing literature on the pore water pressure dissipation method reveals that, while there are some examples of model-based experimental approaches (e.g., Tanaka et al.,

*corresponding author

E-mail address: noda@nagoya-u.jp (T. Noda).

Peer review under responsibility of The Japanese Geotechnical Society.

1984; Unno et al., 2012), there has been essentially no research involving a full-scale numerical analysis of the real ground. This is because there are three major challenges impeding the numerical simulation of the pore water pressure dissipation method. The first and second challenges are closely related to the principle underlying the method. Countermeasures to liquefaction that employ cement treatment or chemical grouting seek to harden the liquefaction-prone layer, and do in fact prevent liquefaction of at least the target layer. Densification methods, exemplified by the sand compaction pile (SCP) method, also increase the liquefaction strength and liquefaction resistance of the treated layer. Meanwhile, as is well known, the pore water dissipation method seeks to prevent liquefaction by suppressing the increase in pore water pressure and does not attempt to improve the mechanical properties or conditions (i.e., to proactively increase the strength or rigidity) of the ground in question. In other words, it is a countermeasure method with the potential for actually causing liquefaction. Thus, simulations must also be able to reproduce liquefaction in cases where the countermeasure does not perform as expected. As mentioned earlier, because it is a method that, when effective, causes compaction, the constitutive equation must be capable of reproducing both compaction and liquefaction in response to external forces. In order to reproduce liquefaction or compaction behavior that is likely to occur during an earthquake, in addition to the settlement due to consolidation, which is especially problematic after liquefaction, the underlying mechanical theory and the numerical analysis method, employed to solve the governing equation, must be able to seamlessly handle deformation and failure behavior during and after an earthquake and to reproduce the effect of partial drainage. Given these requirements, in this research, we employed the SYS Cam-clay elasto-plastic constitutive model based on the soil skeleton structure concept (Asaoka et al., 2002) installed in the *GEOASIA* soil–water coupled finite deformation analysis code (Noda et al., 2008). The SYS Cam-clay model is equally capable of handling liquefaction and compaction as phenomena resulting from the degradation of the structure and the accumulation of over-consolidation, while also accounting for the mechanical behavior of a wide range of ground materials. *GEOASIA* is a soil–water coupled finite element analysis code based on the two-phase mixture theory in the finite deformation regime, and partial drainage effects appear naturally in the analysis results. It integrates the rate-type equation of motion over time, based on an extended Wilson- θ method adopted for the equation. As such, it is capable of consistently handling a wide range of ground deformation and failure behavior (before, during, and after an earthquake) without having to distinguish between quasi-static and dynamic problems.

The third challenge facing the numerical simulation of the pore water pressure dissipation method concerns the difficulty of representing a large number of vertical drains installed in the ground. While the ideal solution would be to represent such drains by increasing the mesh density, this would require a very large number of elements and would not be practical when performing a 3-D analysis. In other words, to be able to

perform a practical simulation of the pore water pressure dissipation method using a numerical analysis code that meets the first two requirements, what is needed is the incorporation of some means of efficiently representing the water absorption and discharge functions of vertical drains. The macro-element method (Sekiguchi et al., 1986; Yamada et al., 2015), which is a type of homogenization method, is frequently employed in effective stress analyzes for consolidation-related problems, which suffer from the same difficulties as those involved in representing vertical drains. In the present study, we attempted to resolve this issue by applying the macro-element method to a dynamic problem, when it had only been applied, up to this point, to quasi-static problems. The method was recently extended by the authors to include the discharge function of vertical drains in addition to the water absorption function that the original macro-element method has (Yamada et al., 2015). In this paper, we attempted to incorporate the macro-element method into the *GEOASIA* soil–water finite deformation analysis code, which is capable of accounting for inertial forces.

In the following sections, we first describe how the macro-element method was introduced to the soil–water finite deformation analysis code with inertia terms. Next, we demonstrate that the macro-element method is capable of generating highly accurate approximations for dynamic problems, using the example of a 3-D unit cell model surrounding a single drain. Furthermore, in order to confirm the effect of suppressing the increase in pore water pressure on reducing deformation, such as lateral flow, we provide an example of numerical calculations conducted for the case of sandy soil directly beneath an embankment, to which the pore water pressure dissipation method is applied as a countermeasure to liquefaction. In addition, with countermeasure design in mind, we briefly discuss approaches for reducing the number of test calculations required for determining the drain spacing and improvement region.

2. Application of macro-element method to soil–water finite deformation analysis code with inertia terms

The soil–water finite deformation analysis with inertia terms, developed by the authors (Noda et al., 2008), employs a so-called *u-p* formulation to obtain the nodal displacement velocity vector $\{\dot{\mathbf{v}}^N\}$ and representative pore water value u for each element by solving the space-discretized rate-type equation of motion and soil–water coupled equation given by:

$$\mathbf{M}\{\ddot{\mathbf{v}}^N\} + \mathbf{K}\{\dot{\mathbf{v}}^N\} - \mathbf{L}^T \dot{u} = \{\dot{\mathbf{f}}\} \quad (1)$$

$$\frac{k}{g} \mathbf{L}\{\dot{\mathbf{v}}^N\} - \mathbf{L}\{\mathbf{v}^N\} = \sum_{i=1}^m \alpha_i (h - h_i) \rho_w g \quad (2)$$

where \mathbf{M} is the mass matrix, \mathbf{K} is the tangent stiffness matrix, \mathbf{L} is the matrix for converting $\{\mathbf{v}^N\}$ to the element volume change rate, $\{\dot{\mathbf{f}}\}$ is the nodal force rate vector, $\{\dot{\mathbf{v}}^N\}$ and $\{\ddot{\mathbf{v}}^N\}$ denote the nodal acceleration and jerk vectors, h and h_i .

represent the total heads corresponding to the representative values for water pressure for an element and adjacent elements, respectively, k is the permeability coefficient for the ground, g is the magnitude of gravitational acceleration, α_i is the coefficient of pore water flow to adjacent elements, ρ_w is the density of water, and m is the number of boundary surfaces for each element. The first term on the left-hand side of Eqs. (1) and (2) is the one which vanishes when the inertia forces do not work. For the sake of simplicity, the compressibility of water has been ignored.

Next, the previously developed macro-element method, with water absorption and discharge functions for vertical drains (Yamada et al., 2015), was applied to the above analytical method. First, we applied the following soil-to-drain pore water flow model to each element:

$$\dot{Q}_D = \kappa(u - u_D) \quad (= \kappa(h - h_D)\rho_w g) \quad (3)$$

$$\kappa = \frac{8kV}{F(n)d_e^2 \rho_w g} \quad (4)$$

$$F(n) = \frac{n^2}{n^2 - 1} \ln n - \frac{3n^2 - 1}{4n^2}, \quad n = \frac{d_e}{d_w} \quad (5)$$

where \dot{Q}_D is the soil-to-drain pore water flow rate, κ is the coefficient of pore water flow from the soil to the drain, u_D is the representative value for water pressure in the drain for each element, h and h_D are the total heads corresponding to u and u_D , respectively, and V is the current volume of each element. d_e and d_w represent the equivalent diameter and diameter of the circular drain, respectively, and are treated as material constants.

To incorporate the water absorption function of vertical drains into each element, Eq. (3) is added to the right-hand side of Eq. (2), yielding the following expression:

$$\frac{k}{g} L\{\dot{v}^N\} - L\{v^N\} = \sum_{i=1}^m \alpha_i (h - h_i) \rho_w g + \kappa (h - h_D) \rho_w g \quad (6)$$

Eq. (6) is called the soil–water continuity equation and replaces Eq. (2) as a governing equation.

In the original formulation of the macro-element method (Sekiguchi et al., 1986), u_D or h_D was specified by the analyst/investigator as an analytical condition. However, the authors recently proposed treating this value as an unknown. The following continuity equation for the drain, which is included virtually in the macro-element, is formulated in order to compensate as many equations as the increased unknowns, on the assumption that the mesh division from the top to the bottom of the improved region is initially divided up approximately vertically:

$$\kappa (h - h_D) \rho_w g = \sum_{j=1}^2 \beta_j (h_D - h_{Dj}) \rho_w g \quad (7)$$

where β_j is the coefficient of water flow through the virtual drain contained in each element, and h_{Dj} is the total head of the drain contained in the elements above and below the macro-element. For the sake of simplicity, it is assumed that water flow through the drain obeys Darcy's law. Bearing in mind that the ratio of the cross-sectional area of the virtual drain to the area of the boundary surface between the elements connected above and below is $1/n^2$, β_j is given by the following equation:

$$\beta_j = \frac{k_w l^j}{l^j l^j} \cdot n^j \frac{s^j}{n^2} \quad (8)$$

where each symbol is defined as illustrated in Fig. 1. k_w is the permeability coefficient for a circular drain and is treated as a material constant. The discharge function of the drains is incorporated in the macro-element method by treating the water pressure in the drain as an unknown, while simultaneously adding Eq. (7) as a governing equation. The boundary conditions for Eq. (7) are handled in the same manner as the hydraulic boundary conditions for Eq. (2). Unless there is a particular reason, the initial value for water pressure in the drain is to be matched with the pore water pressure at the point when the macro-element is applied.

Ultimately, Eqs. (1), (6), and (7) represent the governing equations when the macro-element method is applied. Solving these equations simultaneously yields $\{v^N\}$, u , and u_D . As implied by the fact that Eq. (1) is used as it is, we assume that the effect of the vertical drain's presence on the element's rigidity and mass is negligible, and therefore, can be ignored. In addition, we assume that the change in drain volume in Eqs. (6) and (7) is sufficiently small relative to the change in ground volume, and therefore, can be ignored.

One noteworthy feature of the macro-element method is that the mesh division can be specified independently of the drain arrangement and the drain spacing. As presented in Yamada et al. (2015), the supplementary conditions for the macro-element method proposed by Sekiguchi et al. (1986), (1988) do not apply. For a detailed explanation of how material constants d_e , d_w , and k_w are determined, see (Yamada et al., 2015).

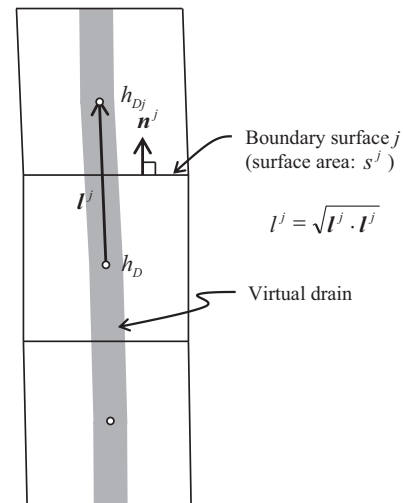


Fig. 1. Virtual drain contained in macro elements.

In addition, in analyzes based on the u - p formulation, there is an upper limit for the permeability coefficient in terms of the time increment per step (Noda et al., 2008). Although this upper limit can hinder calculations when the drain is represented using a divided mesh, the drain permeability coefficient in the macro-element method is not subject to such constraints. In terms of analyzes based on the u - p formulation, this point, along with the improved calculation efficiency, can be cited as merits of the macro-element method.

3. Accuracy of approximations using macro-element method for dynamic problems

The authors demonstrated in a previous research (Yamada et al., 2015) that the macro-element method is also capable of yielding highly accurate approximations for problems involving material and/or geometric non-linearity, or multi-layered grounds. In this section, we confirm the high level of accuracy of approximations when the same approach is applied to dynamic problems.

3.1. Analysis conditions

The analysis was conducted for a 3-D unit cell model surrounding a single drain. The ground to be improved was a 10 m thick loose sandy ground. Two models were constructed: an ‘exact model’, in which the analytical domain was a mesh that was finely divided even in the horizontal direction, and an ‘approximate model’, utilizing the macro-element method, for which the mesh was not divided horizontally. The finite element meshes and boundary conditions adopted in the two models are presented in Figs. 2 and 3, respectively. We assumed drains arranged in a square pattern in a horizontally layered ground at a spacing of 1.0 m and applied a periodic boundary to the sides of the analysis domain. A viscous boundary was applied to the bottom boundary in the horizontal direction (Lysmer and

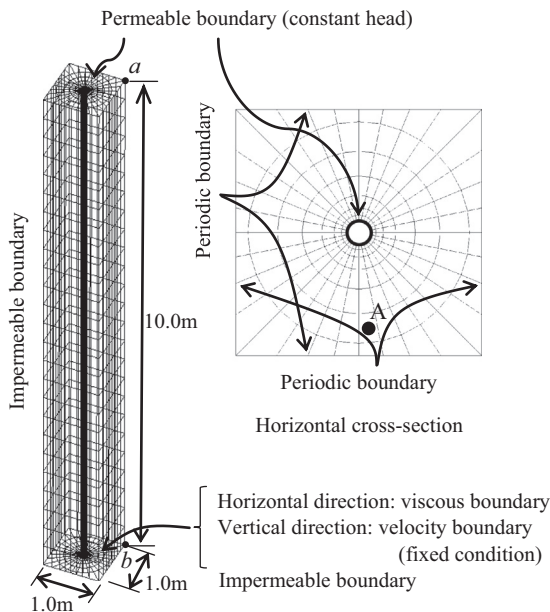


Fig. 2. Finite element mesh and boundary conditions (exact model).

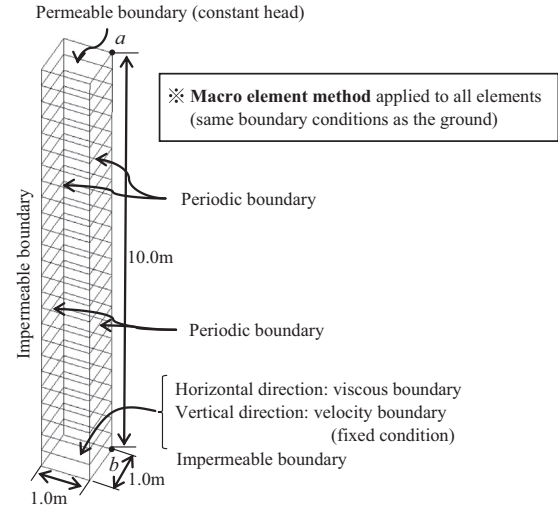


Fig. 3. Finite element mesh and boundary conditions (approximate model).

Table 1

Material constants and initial values for ground and embankment.

	Ground	Embankment
Elasto-plastic parameters		
Critical state index M	1.00	1.35
NCL intercept N	1.98	1.71
Compression index $\tilde{\lambda}$	0.050	0.110
Swelling index $\tilde{\kappa}$	0.016	0.020
Poisson's ratio ν	0.3	0.3
Evolution parameters		
Ratio of $-D_v^p$ to $\ D_s^p\ c_s$	1.0	1.0
Degradation index of structure a	2.20	2.00
Degradation index of OC m	0.10	0.50
Rotational hardening index b_r	3.50	0.10
Limitation of rotational hardening m_b	0.70	0.40
Fundamental parameters		
Soil particle density ρ_s (g/cm ³)	2.65	2.67
Permeability index k (cm/s)	1.0×10^{-3}	1.0×10^{-4}
Initial conditions		
Coefficient of lateral pressure K_0	0.8	0.8
Degree of structure $1/R_0^*$	4.0	1.1
Overconsolidation ratio $1/R_0$	1.2	42.5
Degree of anisotropy ζ_0	0.0	0.0

Kuhleemeyer, 1969; Noda et al. 2009), while a fixed boundary condition was applied in the vertical direction. In terms of the hydraulic boundary conditions, an impermeable condition was applied to both the side and the bottom boundaries. The boundary at the ground surface was initially assigned a water pressure of zero, and later a permeable condition was applied that retained a prescribed head (i.e., the case in which there is standing water). For the vertical drain, we assumed a spiral drain (Research Association for DEPP Method, 2011) with a diameter of 0.1 m and a permeability coefficient of 7.0×10^2 cm/s. In the exact model, the drain part was represented as a cavity, and the part adjacent to the drain, was set to be a permeable boundary with a constant head, similar to the ground surface.

The material constants and initial values adopted for the ground (including values for the embankment used in the next section) are

presented in Table 1. The ground was assumed to be a loose sandy soil that would be prone to liquefaction if not improved. The initial values shown in Table 1 were assigned uniformly to the entire ground. The stress condition was determined by accounting for the ground's own weight under the application of a slight load to the ground surface (9.81 kN/m²). The initial water pressure distribution was hydrostatic. The void ratio was calculated based on the conditional equation that the state variables should satisfy (Noda et al., 2005).

The material constants for the viscous boundary at the bottom of the model and the macro-element are shown in Tables 2 and 3, respectively. Equivalent diameter d_e was specified so that the effective improved area ($\pi d_e^2/4$) was equivalent to the horizontal cross-sectional area of the 3-D unit cell model.

The input ground motion is shown in Fig. 4. This represents a seismic wave of the kind associated with a Tokai–Tonankai–Nankai linked-type earthquake having a main shock duration of 120 s and a maximum acceleration in the order of 180 gal. Excitation occurs in two horizontal directions. The dotted lines in Figs. 4 and 6–9 indicate the times of cessation of ground motion input.

Table 2
Material parameters of viscous boundary.

Bedrock density ρ (g/cm ³)	2.00
S-wave velocity in bedrock V_s (m/s)	150.0

Table 3
Material parameters of macro-element method.

Equivalent diameter d_e (m)	1.13
Diameter of circular drain d_w (m)	0.10
Permeability coefficient of circular drain k_w (cm/s)	7.00×10^2

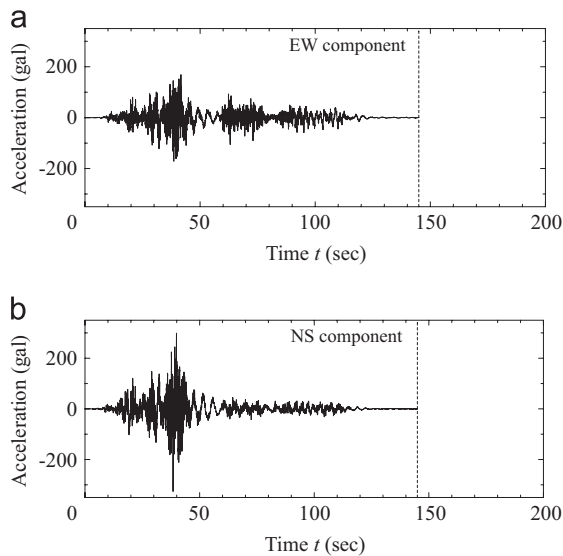


Fig. 4. Input seismic motion.

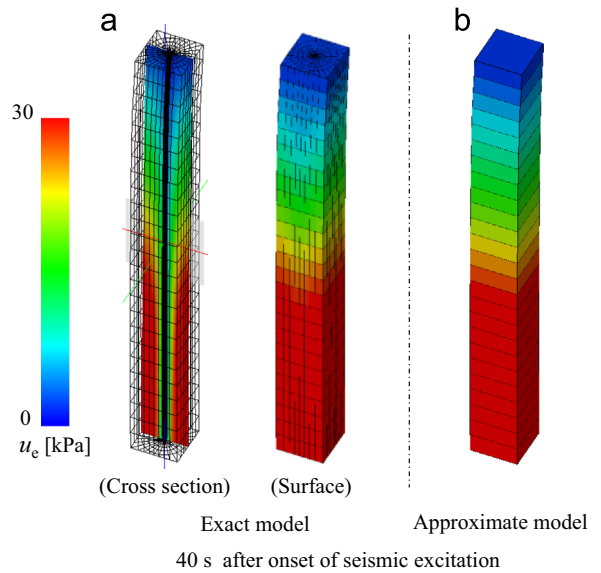


Fig. 5. Distribution of excess pore-water pressure.

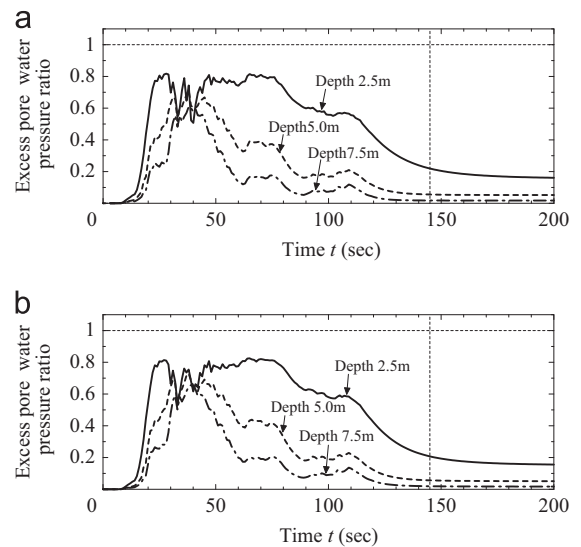


Fig. 6. Time-excess pore water pressure ratio relationship (a) Exact model and (b) Approximate model.

3.2. Analysis results

The excess pore water pressure distribution for each model is shown in Fig. 5. The figure also shows the distribution of the vertical cross section, including the drain for the exact model. Both the exact and the approximate models yielded similar trends for the distributions at the ground surface. In addition, the water pressure appears to be lower in the vicinity of the drain in the exact model. Fig. 6 shows the time-excess pore water pressure ratio relationship for elements that were initially at depths of 2.5, 5.0, and 7.5 m. The upper surface, representing the exact model, shows values for elements at the prescribed depths and at location A in Fig. 2. Following the change in excess pore water pressure ratio over time, it can be

seen that, for these element locations, the approximate model yields essentially the same values for the pressure ratio as the exact model does. Furthermore, in both models, although the excess pore water pressure ratio continues to rise for a period of time after the onset of shaking, it stops rising after reaching a value of 0.8 or so, and therefore, does not reach liquefaction. (Calculations for the same ground without countermeasures resulted in an excess pore water pressure greater than 0.95).

From the above, it can be seen that the approximate model is capable of closely approximating the change in water pressure generated by the exact model, at least for the locations compared in Fig. 6. Meanwhile, because the macro-element method is a type of homogenization method that averages the heterogeneity in the pore water pressure distribution around the vertical drain, as demonstrated in the interior of the exact model (Fig. 5), it does not directly deal with the heterogeneity in the effective stress and state variables similarly arising around the drain, or with the resulting heterogeneity in the rigidity. Next, we set out to determine whether or not the model could accurately approximate the ground response, even if only the average rigidity is treated. Figs. 7 to 9 show the changes with time in the horizontal acceleration of the ground surface, in the horizontal relative displacement to the bottom of the ground, and in the ground surface settlement, respectively. The nodes representing the relevant ground and basement surfaces are identified as points *a* and *b* in Figs. 2 and 3. In all cases, essentially the same response was produced by the exact and approximate models.

Next, we compared the relationship between the mean effective stress and the specific volume in order to investigate the behavior of elements in the ground. The elements used in this comparison were located at a depth of 2.5 m. For the exact model, the element at the prescribed depth, located at point A in Fig. 2, was used. As shown in Fig. 10, both elements exhibit very similar behavior. The mean effective stress falls, at the very

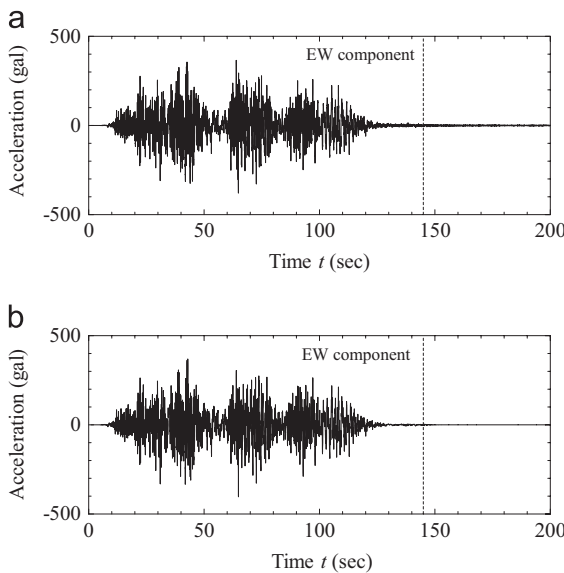


Fig. 7. Acceleration response (a) Exact model and (b) Approximate model.

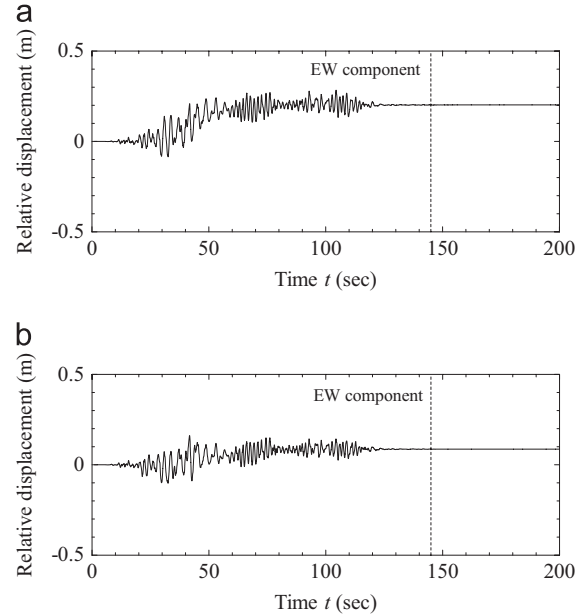


Fig. 8. Relative displacement response (a) Exact model and (b) Approximate model.

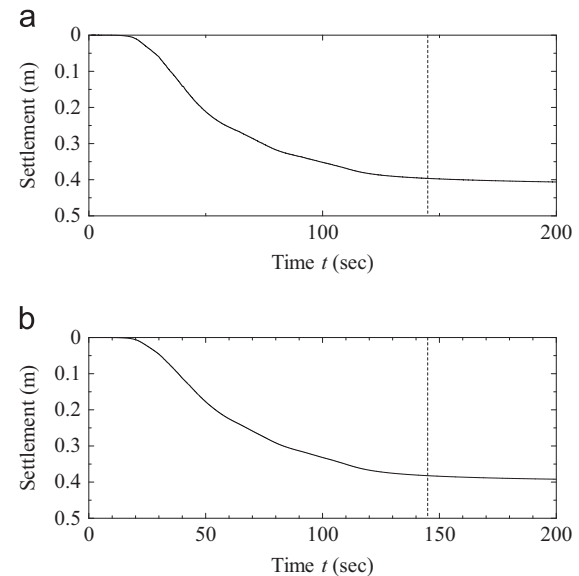


Fig. 9. Settlement behavior (a) Exact model and (b) Approximate model.

most, to approximately 2/3 of the original value. On the other hand, compression due to compaction occurs during the earthquake. Furthermore, very little compression due to consolidation appears to occur after seismic activity ends. Thus, the suppression of the increase in pore water pressure, attributable to the water absorption function of the vertical drains and the ground compaction that occurs in its place, can be reproduced by the numerical calculations. As mentioned above, the macro-element method is highly effective for approximating the water absorption and discharge functions of vertical drains. Meanwhile, it should be recognized that it is the SYS Cam-clay model and the **GEOASIA** code that allow the reproduction of the compaction behavior and the dynamic calculation.

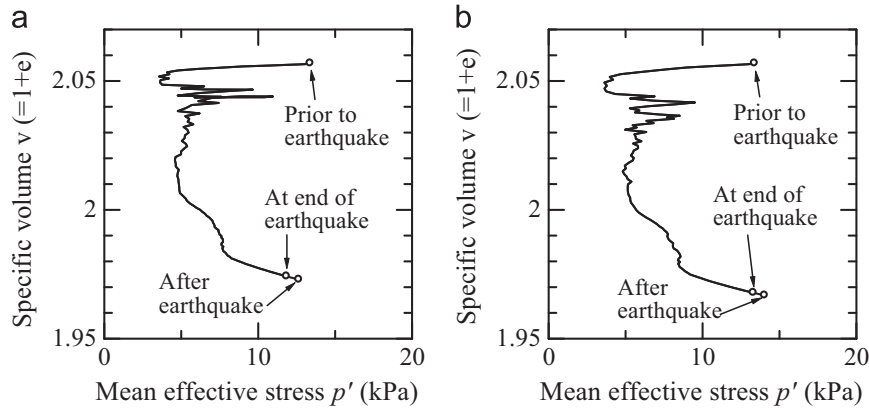


Fig. 10. Compaction behavior during earthquake (a) Exact model and (b) Approximate model.

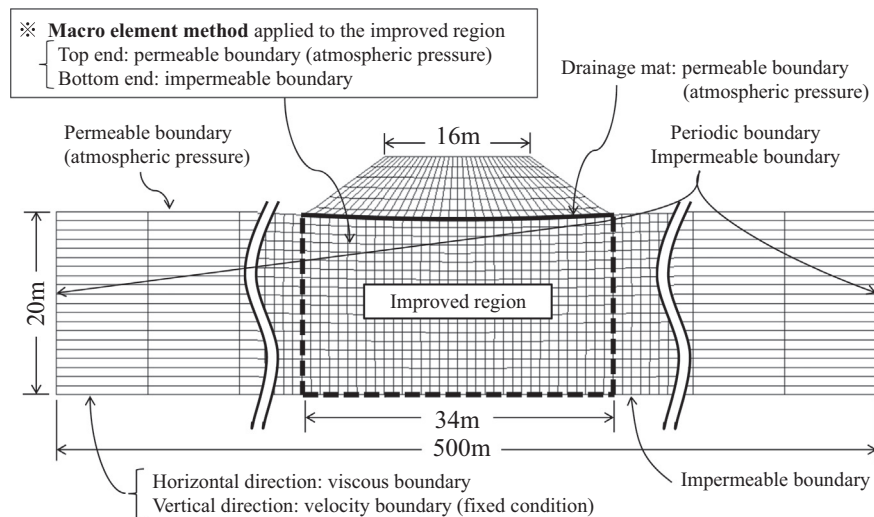


Fig. 11. Finite element mesh and boundary conditions (2-D mesh).

4. Calculation example of improvement effect for excess pore water pressure dissipation method

Next, in order to confirm the effect of suppressing the increase in pore water pressure on inhibiting ground deformation, such as lateral flow, we describe calculations for the case where liquefaction countermeasures, based on the pore water pressure dissipation method, are applied to a sandy ground directly beneath an embankment. In addition, with an appropriate countermeasure design in mind, we briefly discuss ways of employing a 1-D mesh to reduce the number of cases in which calculations using 2-D and 3-D meshes are required when examining the drain spacing and the improved region.

4.1. Analysis conditions

The finite element mesh and the boundary conditions adopted here are shown in Fig. 11. Plane strain conditions were assumed. The ground directly under the embankment was designated as the improved region, and the macro-element method was applied to its relevant parts. Since the radial water flow around a vertical drain is functionally assumed in the

macro-element method, the effect of water absorption is evaluated appropriately corresponding to the specified drain arrangement and spacing even if under plane strain conditions. A high-permeability drainage mat was assumed to be laid between the embankment and the ground, and a permeable boundary (atmospheric pressure) was assigned to the embankment-ground interface. A periodic boundary was applied to the vertical sides of the ground, while a viscous boundary was applied to the bottom boundary in the horizontal direction. Table 1 presents the material constants and initial values for the ground, Table 2 shows the material constants of the viscous boundary, and Table 3 gives the material constants for the macro-element method. An embankment with a final height of 6 m was added to the horizontally layered ground over a period of 18 days (Takaine et al., 2010), and the consolidation was calculated until a steady state was achieved. Next, the EW component of the ground motion used in the calculations in the previous section was applied to this embankment-ground system, and consolidation was allowed to proceed until the excess pore water pressure had completely dissipated. Naturally, both the quasi-static and the dynamic processes in the period extending from before the earthquake had started to

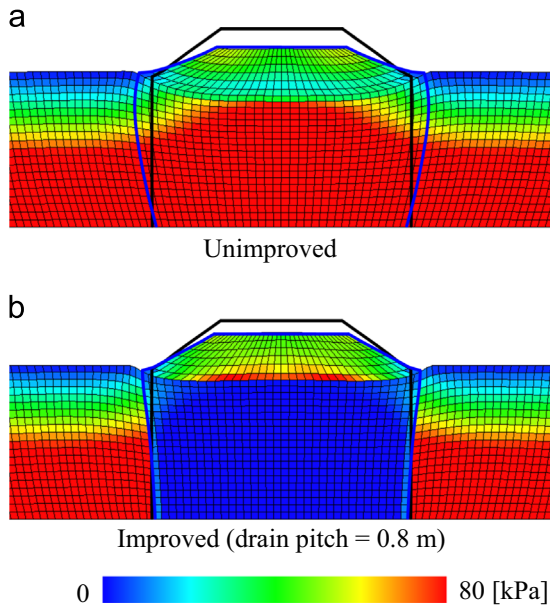


Fig. 12. Distribution of excess pore water pressure after end of seismic motion.

after it had finished were consistently calculated with a single analysis code.

4.2. Analysis results

Fig. 12(a) and (b) show the pore water pressure distribution immediately following the cessation of ground motion for cases of an unimproved ground and a ground with a drain spacing of 0.8 m, respectively. In order to make the deformation easier to see, a thick line has been drawn in the figures demarking the sides of the improvement region and the embankment perimeter prior to the earthquake. Using the macro-element method, the effect of the pore water pressure dissipation method on suppressing the increase in water pressure becomes readily apparent in the analysis results. Lateral flow and settlement of the ground directly beneath the embankment are clearly reduced, in addition to deformation of the embankment itself. When no countermeasures are applied, large-scale lateral flow of the ground occurs as a result of the reduction in shear stiffness as the effective stress approaches the origin along with the increase in water pressure. In contrast, when the countermeasures are applied, the decrease in effective stress is halted, which in turn inhibits the reduction in the shear stiffness of the ground, thereby decreasing the lateral flow and accompanying settlement. Fig. 13 shows the dependence of the rates of water pressure increase, settlement, and lateral flow, as defined below, on the drain spacing.

[Water pressure increase rate]=[maximum pore water pressure with ground improvement]/[maximum pore water pressure without ground improvement].

[Settlement rate]=[final settlement at the embankment crown center with ground improvement]/[final settlement at the embankment crown center without ground improvement].

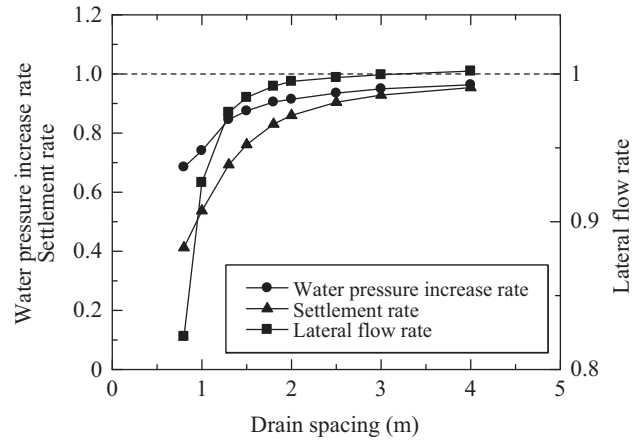


Fig. 13. Relationship between drain spacing and improvement effects.

[Lateral flow rate]=[final width of embankment bottom with ground improvement]/[final width of embankment bottom without ground improvement].

The settlement rate and the lateral flow rate include the amount of deformation due to the consolidation processes that occur after the earthquake. By reducing the drain spacing, deformation, such as settlement and lateral flow, can be sufficiently suppressed to inhibit the increase in pore water pressure. For the analysis conditions in this study, the effect of the drain starts to appear at a spacing of approximately 2.0 m, and increases as the spacing falls below 1.0 m.

4.3. Proposal of efficient design procedure on improved effect using 1-D mesh-based analysis

As mentioned in the Introduction, because the pore water pressure dissipation method allows for a certain degree of deformation, when determining drain spacing and the improved region, the prediction of the amount of deformation is essential. The above results suggest that an effective stress analysis with improved calculation efficiency, by means of introducing the macro-element method, is a promising approach to achieving this goal. At the same time, although the calculation efficiency is improved through the application of the macro-element method, it is still desirable to limit the number of test cases as much as possible. As can be seen in Fig. 13, because only a limited range in drain spacing is actually effective, it is possible to refine the number of cases calculated as long as the range in effective drain spacing is ascertained beforehand. The other important point illustrated in Fig. 13, which may be obvious from the underlying principle of this particular ground-improvement method, is the strong correlation between the suppression of the increase in pore water pressure and the inhibition of deformation. Although 2-D or 3-D mesh-based analyzes are necessary for detailed predictions of deformation, an analysis using a 1-D mesh could possibly be sufficient for capturing the effects of the suppression of the increase in pore water pressure, assuming that this is the sole aim of the endeavor. Therefore, we investigated the

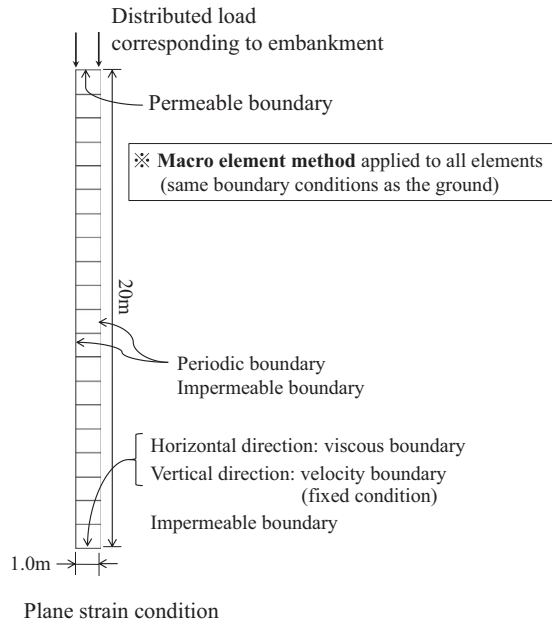


Fig. 14. Finite element mesh and boundary conditions (1-D mesh).

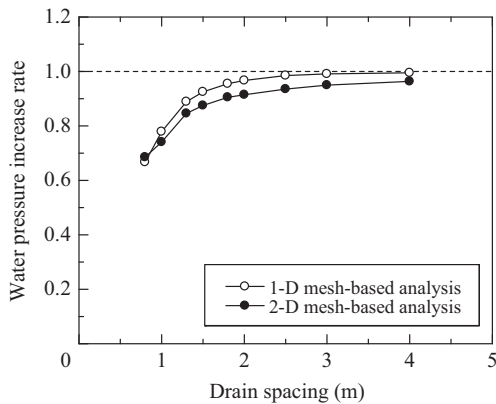


Fig. 15. Relationship between drain spacing and suppression of water pressure increase (comparison of 1-D and 2-D mesh based analyses).

relationship between drain spacing and the suppression of the increase in pore water pressure via the 1-D mesh-based analysis shown in Fig. 14. The analysis conditions are as shown in the figure, and the material constants and the initial values for the ground were the same as those used in the 2-D mesh-based analysis. However, for simplicity, in the 1-D mesh-based analysis, the presence of the embankment was accounted for by adding a distributed load to the ground surface. The 1-D mesh-based analysis results are shown together with the results of the 2-D mesh-based analysis in Fig. 15. It is evident that very similar relationships between the drain spacing and the suppression of the increase in pore water pressure were obtained by the 1-D and 2-D mesh-based analyses. Thus, it can be concluded that the design process can be further streamlined by first performing a 1-D mesh-based analysis to determine the range in effective drain spacing, prior to performing 2-D or 3-D mesh-based analyses.

5. Conclusion

In this study, a simulation of the pore water pressure dissipation method was conducted by incorporating a macro-element method, which had previously only been applied to quasi-static problems, to the *GEOASIA* soil–water finite deformation analysis code together with the elasto-plastic constitutive SYS Cam-clay model based on the soil skeleton structure concept. The main findings are as follows:

1. The macro-element method is capable of yielding highly accurate approximations even for dynamic problems.
2. The macro-element method enables the effect of the suppression of the increase in pore water pressure, associated with the pore water dissipation method, to be reproduced even when a relatively coarse mesh is used.
3. The same analytical method is capable of reproducing the effect of the reduction of the loss in shear stiffness (and the resulting reduction in lateral displacement and settlement), which is due to the suppression of the decrease in effective stress.
4. The design procedure for the pore water pressure dissipation method can be streamlined by first determining the range in effective drain spacing using a 1-D mesh-based analysis, prior to performing 2-D and 3-D mesh-based analyses.

In addition, although this did not arise in the calculations carried out in the present study, because the macro-element method proposed by the authors' research group treats water pressure in the drain as an unknown, it is capable of treating cases of drainage stagnation and liquefaction that result from the insufficient discharge capacity of vertical drains. Furthermore, because the macro-element method formulated by the authors does not require mesh division to be matched to drain spacing, it is possible, as demonstrated in this study, to investigate the effect of different intervals of drain spacing using the same mesh. This is another notable advantage of using the macro-element method.

As partially demonstrated above, the adoption of the macro-element method extends the range of engineering problems to which *GEOASIA* can be applied. It is expected that the value of using the macro-element method will increase with the simulation scale. Meanwhile, in terms of simulating the pore water pressure dissipation method, the ability to reproduce the increase in pore water pressure due to seismic motion, and the inhibition of deformation due to suppressing this increase, depends on the effectiveness of the analysis code to which the macro-element method is applied. In other words, the macro-element method is useful but, in the end, is simply a tool. For its utility to be leveraged, the analysis code must be effective at its core. As the next step, we hope to extend the value of the macro-element method by comparing simulation and experimental results and by improving the constitutive equation.

Acknowledgments

This paper reports on research carried out by the Technical Committee for the Mechanisms of Earthquake-Induced

Ground Deformations (Chairman Akira Asaoka), a committee for seismic response research operating under the Japanese Geotechnical Society. In addition, this work was supported by JSPS KAKENHI Grant numbers 21226012 and 25249064.

References

- Asaoka, A., Noda, T., Yamada, E., Kaneda, K., Nakano, M., 2002. An elasto-plastic description of two distinct volume change mechanisms of soils. *Soils Found.* **42** (5), 47–57.
- Lysmer, J., Kuhlemeyer, R.L., 1969. Finite dynamic model for infinite media. *ASCE. J. Eng. Mech.* **95** (4), 859–877.
- Noda, T., Asaoka, A., Yamada, S., 2005. Elasto-plastic behavior of naturally deposited clay during/after sampling. *Soils Found.* **45** (1), 51–64.
- Noda, T., Asaoka, A., Nakano, M., 2008. Soil-water coupled finite deformation analysis based on a rate-type equation of motion incorporating the SYS Cam-slay model. *Soils Found.* **45** (6), 771–790.
- Noda, T., Takeuchi, H., Nakai, K., Asaoka, A., 2009. Co-seismic and post-seismic behavior of an alternately layered sand-clay ground and embankment system accompanied by soil disturbance. *Soils Found.* **49** (5), 739–756.
- H. Sekiguchi T. Shibata A. Fujimoto H. Yamaguchi. A macro-element approach to analyzing the plane strain behavior of soft foundation with vertical drains. In: *Proceedings of the 31st Symposium of the JGS 1986*. pp. 111–116.
- Sekiguchi, H., Shibata, T., Mimura, M., Sumikura, K., 1988. Behaviour of the seawall and bridge abutment at the edge of an offshore airport fill. *Ann., Disas. Prev. Res. Inst., Kyoto Univ.* **32** (B-2), 123–145.
- Y. Tanaka T. Kokusho Y. Esashi I. Matsui, On preventing liquefaction of level ground using gravel piles . In: *Proceedings of the JSCE, III-2, 352, 2,1984*, pp. 89–98.
- Unno, T., Hayashi, K., Asada, H., Iba, H., 2012. Evaluation of the dissipation of excess pore water pressure method using centrifugal model test. *Proc. JSCE B3 68* (2), I_480–I_485.
- Yamada, S., Noda, T., Tashiro, M., Nguyen, H.S., 2015. Macro-element method with water absorption and discharge functions for vertical drains. *Soils Found.* **55** (5), 1113–1128.
- Research Association for DEPP Method Technical data on dissipation of excess pore water pressure method 2011.
- Takaine, T., Tashiro, M., Shiina, T., Noda, T., Asaoka, A., 2010. Predictive simulation of deformation and failure of peat-calcareous soil layered ground due to multistage test embankment loading. *Soils Found.* **50** (2), 245–260.